Topotactic Intercalation of a Metallic Dense Host Matrix Chalcogenide with Large Electron-Phonon Coupling: Crystal Structures and Electronic Properties of $Li_xMo_2SbS_2$ ($0 \leq x < 0.7$)

Alexandros Lappas[a,*], Christopher J. Nuttall[a], Zacharias G. Fthenakis[a], Vladimir Yu. Pomjakushin[b], and Mark A. Roberts[c]

[a] *Institute of Electronic Structure and Laser, Foundation for Research and Technology – Hellas, P.O. Box 1527, 711 10 Herakion, Crete, Greece.*

[b] *Laboratory for Neutron Scattering ETHZ & PSI, CH-5232 Villigen PSI, Switzerland.*

[c] *Synchrotron Radiation Source, Daresbury Laboratory, Warrington WA4 4AD, Cheshire, UK.*

[*] Corresponding author. E-mail: lappas@iesl.forth.gr

Supporting Information

Appendix I. Electronic property measurements setup

A temperature controlled continuous flow cryostat and a nano-voltmeter (Agilent 34420A) were the key components of the home-made computer controlled setup for conductivity measurements. Cold-pressed polycrystalline materials were cut from Ø10 mm, 1 mm thick pellets into rectangular shaped bars inside the glove-box. Electrical contacts on the sample surface were made by using Cu wire with conducting carbon paste. $Li_xMo_2SbS_2$ samples kept inside the glove-box were placed within screw-cap brass containers equipped with a vacuum tight feed-through for the four-probe leads of the conductivity measurement setup. Furthermore, each container was sealed with Stycast epoxy before being taken to the conductivity apparatus. The estimated error in the absolute value of the electrical resistivity, due to uncertainty in the sample geometry and measuring technique, was ~5%.

For high-pressure *dc* conductivity and *ac* susceptibility experiments, we used a piston-cylinder CuBe clamp cell (I.D. 6 mm) achieving pressures as high as 2 GPa. The pressure transmitting fluid was a 50:50 mixture of FC70/FC77 providing hydrostatic conditions, while the pressure was read by four-probe resistivity measurement of a manganin wire. Having measured the pressure-dependence of the superconducting critical temperature for a piece of 99.999% pure Pb metal by $\chi_{ac}(T)$ (lock-in technique), we were able to calibrate the pressure loss within the cell when we were at cryogenic temperatures. An average pressure drop of about 0.3 GPa was found when the 4.5 K point was reached.

Appendix IIa. Technical aspects of DFT calculations

The DFT calculations with the CASTEP code were pursued on the following basis: (a) an ultra-soft pseudopotential description of the electron-ion interactions represented in the reciprocal space (b) a super-cell approach, with an 1×1×1 repeated unit cell (c) a finite plane wave basis set with its corrections[I] for the description of the wavefunction, truncated with a cut-off energy of 400 eV (d) a fast-Fourier transform (FFT) for the evaluation of the Hamiltonian terms, with a FFT grid of 12×12×12 divisions in the reciprocal space unit cell and (e) an iterative scheme for the self-consistent electronic minimization, using a convergence tolerance of 0.5×10^{-6} eV/atom. For the geometry optimization of the crystal structures, the Broyden - Fletcher - Goldfarb - Shanno (BFGS) algorithm[II] was applied, with the following convergent tolerances: (i) for the changes in energy $\Delta E= 5\times10^{-6}$ eV/atom (ii) for the maximum force 0.01 eV/Å and (iii) for the maximum displacement 5×10^{-4} Å. When the unit cell optimization was necessary, another tolerance criterion was applied for the maximum stress, namely 0.02 GPa.

The DOS calculations incorporated a 5×10×4 Monkhorst-Pack[III] *k*-vector grid for the irreducible part of the first Brillouin zone, while the band structure was calculated along special directions Y Γ Z Δ B Γ of the Brillouin zone, with a 28 *k*-vectors set. For ease of comparison, the *k*-space pathway was chosen to be the same as that utilized previously (see reference 15, in main manuscript), when the electronic structure of the Mo_2SbS_2 was derived with the tight-binding linear muffin tin orbital (TB-LMTO) method.

[I] Milman, V.; Lee, M.H.; Payne, M.C. *Phys. Rev.* B **1994**, *49*, 16300.

[II] Fletcher, R. *Practical Methods of Optimization*; Wiley and Sons: Chichester, 1987.

Appendix IIb. Electronic structure calculation for a solid-solution

In order to access the evolution of the band structure and the density of states (DOS) $N_x(E)$ for the $Li_xMo_2SbS_2$ *solid-solution* we have employed a linear interpolation scheme between the DOS of the Mo_2SbS_2 , $N_0(E) = \sum_i \delta\left(E - E_i^0(x)\right)$, and the DOS of the $LiMo_2SbS_2$, $N_1(E) = \sum_i \delta\left(E - E_i^1(x)\right)$, optimum crystalline structures:

$$N_x(E) = xN_1(E) + (1-x)N_0(E)\,. \qquad (1)$$

$E_i^0(x)$ and $E_i^1(x)$ denote the *i*-th eigenenergy of the corresponding periodic Hamlitonian modified to take into account the new structural details imposed by Li intercalation. However, the knowledge of the $E_i^0(x)$ and $E_i^1(x)$ as a function of the concentration *x*, is limited because of the loss of periodicity, which makes inadequate the calculation for the atomic rearrangement in every intercalated $Li_xMo_2SbS_2$ derivative. To a first approximation the eigenvalues could be approached with those for the two end-members, i.e. $E_i^0(0)$ and $E_i^1(1)$, which are easily calculated from the fully optimized (i.e. unit cell dimensions and atomic arrangement) Mo_2SbS_2 and $LiMo_2SbS_2$ ordered structures. In this nomenclature, $E_i^0(0)$ (or $E_i^1(1)$), the subscript indicates the *i*-th eigenvalue and the superscript points that this calculation was undertaken for the structure of Mo_2SbS_2 (or $LiMo_2SbS_2$); in brackets the concentration, *x*= 0 (or *x*= 1), of lithium intercalant is shown.

[III] Monkhorst, H.J.; Pack, J.D. *Phys. Rev.* B **1976**, *13*, 5188.

For a better estimation of the $E_i^0(x)$ or $E_i^1(x)$ we pursued a linear interpolation between the end-values arising from each end-member structure, namely: $E_i^0(x) = xE_i^0(1) + (1-x)E_i^0(0)$ or $E_i^1(x) = xE_i^1(1) + (1-x)E_i^1(0)$. We calculated the $E_i^0(1)$ and $E_i^1(0)$ assuming a rigid cell size with lattice dimensions fixed to those of Mo_2SbS_2 and $LiMo_2SbS_2$ crystals, respectively. Importantly, full optimization of the atomic positions was undertaken, when lithium was assumed to be inserted (x= 1) or removed (x= 0) from each structure. This modeling permitted us to estimate the effects of the *chemical pressure* (exerted by Li insertion) on the eigenvalues and consequently to the DOS. As a result the DOS $N_x(E)$ for any stoichiometry x of Li, is now written as:

$$N_x(E) = x\sum_i \delta\left(E - xE_i^1(1) - (1-x)E_i^1(0)\right) + (1-x)\sum_i \delta\left(E - xE_i^0(1) - (1-x)E_i^0(0)\right). \quad (2)$$

Because of the small number of eigenvalues used to calculate the DOS, the "delta" functions $\delta(E - E_i)$ which appear in the previous expression were replaced by Gaussian functions of the form $e^{(E-E_i)/2\sigma^2}/\sqrt{2\pi\sigma}$, with $\sigma = 0.05\,\text{eV}$. The result is a smoothed DOS as one would expect for the summation of an infinite number of k-point eigenenergies.

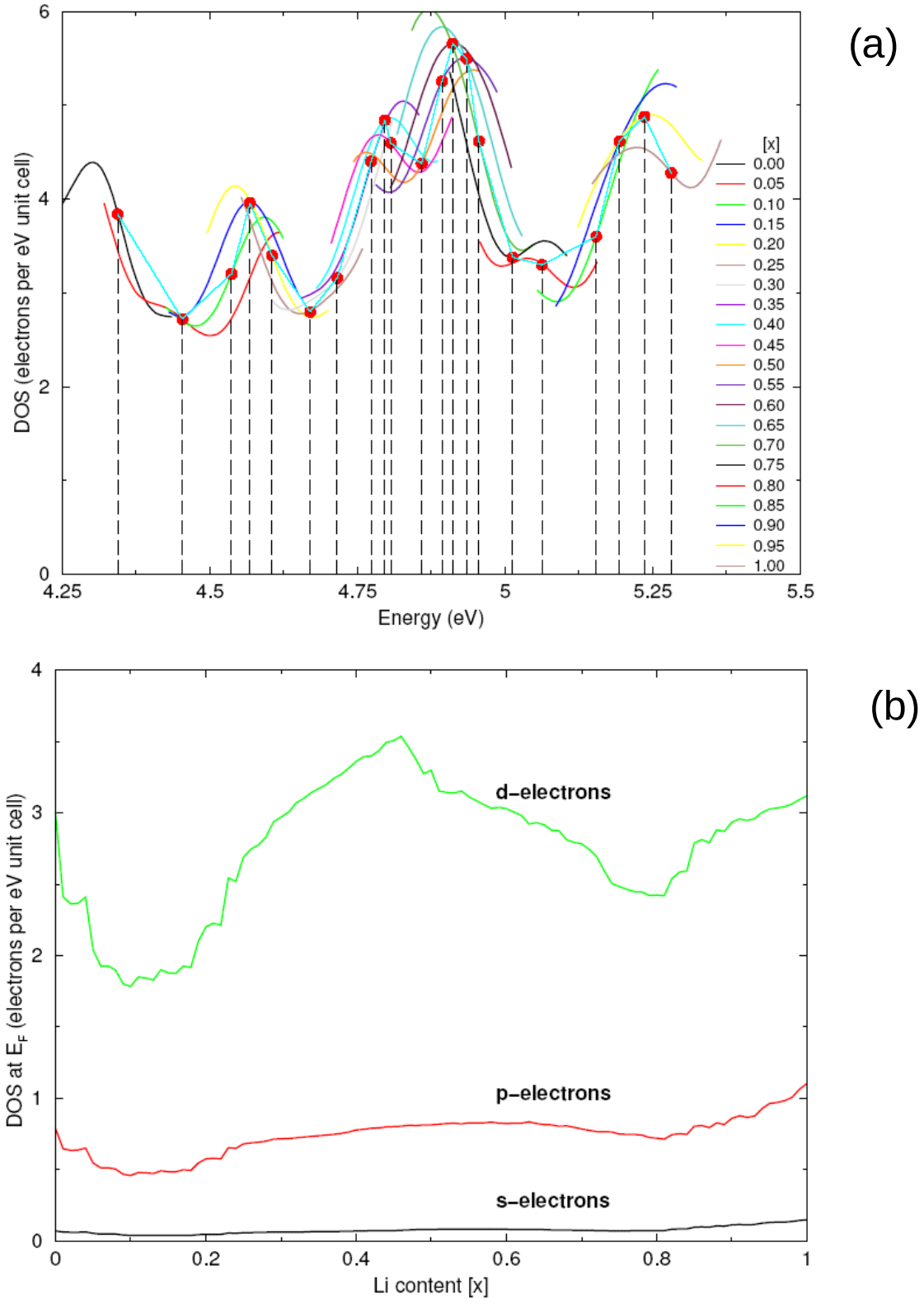

Figure S1. (a) The evolution of the total density of states (DOS) around the Fermi level for various Li *x* compositions. (b) The projected DOS at E_F per orbital versus Li content *x*.

Appendix III. Synchrotron X-ray experiments and predicted structures

Additional information on the effects of the Li-intercalation in the Mo_2SbS_2 structure deduced from the room temperature Rietveld refinements of the $Li_xMo_2SbS_2$ synchrotron X-ray data. Initial refinable variables involved the scale factor, zero point correction, the background function (24-term Chebyschev polynomial), Gaussian and Lorentzian broadening parameters relating to the peak shape function (pseudo-Voigt including peak asymmetry correction), an overall isotropic temperature factor. Having refined the cell parameters and the fractional coordinates of all atoms except those corresponding to the Li (it was kept fixed to the site resolved by neutron powder diffraction), we stopped refining the background coefficients and allowed for the variation of the Li-site occupancy. A representative synchrotron X-ray diffraction profile, for the heavily-doped derivative, namely the $Li_{0.69(3)}Mo_2SbS_2$ material, is shown in Figure 3. It was refined well (χ^2= 6.381, R_{wp}= 4.93%) in a monoclinic $P2_1/m$ structure similar to that adopted by the parent material. However, no $LiNH_2$ impurity was detected in the higher-resolution synchrotron X-ray powder pattern. Crystallographic parameters are compiled in Table S1 and selected bond distances in Table S2. The Li composition, *x*, was extracted on the basis of such refinements and utilized to plot the evolution of the cell parameters (inset to Figure 3) for each sample made for this work.

Composition		Mo_2SbS_2	$Li_{0.69(3)}Mo_2SbS_2$	$LiMo_2SbS_2$
Volume fraction		*theory*	100%	*theory*
T			300 K	
Scan duration			12 hr	
	a /Å	6.5508	6.5834(2)	6.6088
	b /Å	3.1763	3.18518(8)	3.2132
	c /Å	9.3329	9.5278(3)	9.5210
	β /deg	105.316	105.020(1)	103.1676
	V /Å^3	187.296	192.966(14)	196.867
Mo(1)	*x*	0.6633	0.6652(2)	0.6684
	z	0.4791	0.4800(1)	0.4836
	B_{iso} /Å^2		0.160(7)	
Mo(2)	*x*	0.8941	0.8973(2)	0.9120
	z	0.8844	0.8811(1)	0.8783
	B_{iso} /Å^2		0.160(7)	
S(1)	*x*	0.5265	0.5262(6)	0.5098
	z	0.6906	0.6875(4)	0.6849
	B_{iso} /Å^2		0.160(7)	
S(2)	*x*	0.2617	0.2631(5)	0.2598
	z	0.9898	0.9925(4)	1.0047
	B_{iso} /Å^2		0.160(7)	
Sb	*x*	1.0006	0.0028(2)	1.0105
	z	0.3414	0.3423(1)	0.3490
	B_{iso} /Å^2		0.160(7)	
Li	*x*		0.612	0.6219
	z		0.144	0.1593
R_{wp} %, R_p %			4.88, 3.80	
χ^2 , 2θ /deg			6.33 , 3.9-61°	
N-P+C, P, R			5720, 33, 411	

Table S1. Rietveld refined crystallographic parameters of the room-temperature synchrotron X-ray data for the highest Li-content intercalated derivative. The predicted structural parameters of Mo_2SbS_2 and its fully lithiated derivative, $LiMo_2SbS_2$ are also shown for comparison.

T		Mo_2SbS_2 *theory*	$Li_{0.69(3)}Mo_2SbS_2$ 300 K	$LiMo_2SbS_2$ *theory*
Mo(1)	Mo(1)	3.1763	3.18518(8) ×2	3.2132
		2.7737	2.802(2) ×2	2.8191
	Sb	2.8341	2.858(2)	2.8414
		2.8684	2.875(1) ×2	2.8428
	S(1)	2.3736	2.386(4)	2.3839
		2.3527	2.372(3) ×2	2.3835
Mo(2)	Mo(2)	3.1763	3.18518(8) ×2	3.2132
		2.7418	2.813(2) ×2	2.8421
	Sb	2.8656	2.867(1) ×2	2.8343
	S(1)	2.6019	2.652(4)	2.8677
	S(2)	2.3486	2.367(4)	2.3337
		2.3611	2.401(3) ×2	2.3811
Sb	Sb	3.1763	3.18518(8) ×2	3.2132
		3.3606	3.410(2) ×2	3.3235
Li	Mo(1)		3.132(1)	3.0330
	Mo(2)		3.665(1) ×4	3.6286
			3.494(1)	3.5636
	Sb		2.770(1)	2.7831
	S(1)		2.592(3) ×2	2.5132
	S(2)		2.332(3) ×2	2.4760
			2.375(3)	2.4899

Table S2. Selected bond lengths in Å for the intercalated derivative with the highest Li content; parameters were derived after Rietveld refinements of the room-temperature synchrotron X-ray data. Also shown for comparison are bonds derived from the theoretically predicted Mo_2SbS_2 and $LiMo_2SbS_2$ structures.

x		Layer Connectivity			Chain Connectivity					Li-coordination		
Refined	**Nominal**			**In-plane**			**Out-of-plane**		**In-chain**			
		Mo(1)-Mo(1)	Mo(1)-Ŝ(1)-Mo(1)	Mo(1)-Sb	Mo(2)-Mo(2)	Mo(2)-Ŝ(2)-Mo(2)	Mo(2)-Sb	Mo(2)-S(1)	Mo(2)-S(2)	Li-Sb	Li-S(1)	Li-S(2)
0	0	2.768(3) ×2	71.7(2)	2.825(4)	2.748(2) ×2	70.90(19)	2.855(3) ×2	2.618(6)	2.354(5)	--	--	--
		3.18412(8) ×2		2.878(3) ×2					2.384(5) ×2			
0.068(29)	0.2	2.772(2) ×2	72.06(10)	2.829(2)	2.743(2) ×2	70.76(9)	2.853(1) ×2	2.616(4)	2.350(3)	2.6759(9)	2.549(3) ×2	2.277(3) ×2
		3.18163(8) ×2		2.876(1) ×2					2.386(3) ×2			2.345(3)
0.128(29)	0.4	2.776(2) ×2	72.19(10)	2.832(2)	2.760(2) ×2	71.57(9)	2.854(1) ×2	2.618(4)	2.344(3)	2.6925(9)	2.561(3) ×2	2.297(3) ×2
		3.17992(8) ×2		2.879(1) ×2					2.375(3) ×2			2.358(3)
0.190(35)	0.6	2.785(2) ×2	72.38(13)	2.839(2)	2.778(2) ×2	71.49(11)	2.859(2) ×2	2.629(4)	2.359(4)	2.7139(11)	2.576(4) ×2	2.294(3) ×2
		3.17986(9)		2.880(1) ×2					2.395(3) ×2			2.363(4)
0.336(36)	1.0	2.794(3) ×2	72.67(14)	2.853(2)	2.794(3) ×2	72.12(12)	2.863(2) ×2	2.647(5)	2.352(4)	2.7523(12)	2.599(4) ×2	2.318(4) ×2
		3.18102(12) ×2		2.871(2) ×2					2.395(4) ×2			2.379(4)
0.694(29)	0.8	2.802(2) ×2	72.16(11)	2.858(2)	2.813(2) ×2	72.32(10)	2.867(1) ×2	2.652(4)	2.367(4)	2.7696(10)	2.592(3) ×2	2.332(3) ×2
		3.18518(8) ×2		2.875(1) ×2					2.401(3) ×2			2.375(3)

Table S3. Selected bond lengths in Å and angles in deg for $Li_xMo_2SbS_2$ compositions as derived from Rietveld refinements of the room temperature synchrotron X-ray diffraction data; results for the parent (x= 0) are from the 270 K NPD data refinements.

Appendix IV. Mulliken population analyses: electron charge transfer and size effects

Mulliken population analysis shows that upon lithiation there is modification in the electron occupancy for each orbital. A measure of the per formula unit changes is given in Table S4 by the quantity $\Delta\eta = \eta_f - \eta_i$, where η_i and η_f correspond to the Mulliken populations per formula unit of the parent and intercalated compounds, respectively.

The crystal structure determination suggests that lattice expansion arising from *size* effects due to Li insertion may not be the only reason behind the observed changes in the DOS, as Li doping can give rise to *electronic* effects that can act in a coordinated way. It is worthwhile then to understand if one of the two factors plays a dominant role in determining the changes in the DOS for the $Li_xMo_2SbS_2$ system. For this purpose we have calculated the electron counts for the $LiMo_2SbS_2$ structure, however assuming a scenario where the two valence electrons (per unit cell) of Li are not added to the bands. When we compared this to the case of Mo_2SbS_2 we find that the electrons up to the new E_F (= 4.83 eV) are redistributed in such a way that balance their numbers (Table S4). Namely, the *d*- and the *s*- electron counts per unit cell decrease - representing *d* and *s* holes - by 1.24 and 0.50 respectively, while the *p*-contribution increases by 1.74 electrons. Furthermore, to assess how the electron states between the two Fermi levels would be populated by doping with Li (i.e. when one adds back the two electrons to the $LiMo_2SbS_2$; Table S4) our accounting indicates that 1.48 electrons go into *d*-, 0.42 into *p*- and 0.10 into *s*- orbitals. This indicates that despite the electron redistribution which takes place in the inner part of the valence band, a major effect of the presence of Li in the Mo_2SbS_2 structure is the filling of the

d-holes which appear close to the Fermi level region. Let us now consider the optimized model structures of $LiMo_2SbS_2$ and Mo_2SbS_2, which have a rigid cell size (Appendix IIb, in Supporting Information) with lattice dimensions fixed to those of (*compressed* lattice case) Mo_2SbS_2 and (*swollen* lattice case) $LiMo_2SbS_2$ crystals, respectively. The Mulliken population analysis demonstrates no significant changes with respect to the equilibrium $LiMo_2SbS_2$ and Mo_2SbS_2 structures, correspondingly. This test provides some confidence that the size-changes of the unit cell play a limited role in determining the modifications in the DOS of $Li_xMo_2SbS_2$.

Crystal	Mo_2SbS_2 (η_i)					$LiMo_2SbS_2$ (η_f)					
Sites	*s*	*p*	*d*	Total	Charge δ	*s*, Δη	*p*, Δη	*d*, Δη	Total	Δη	Charge δ
S(1)	1.79	4.18	-	5.97	0.03	1.79, 0.00	4.31, 0.13	-	6.09	0.12	-0.09
S(2)	1.84	4.13	-	5.97	0.03	1.79, -0.05	4.38, 0.25	-	6.17	0.20	-0.17
Mo(1)	0.45	0.70	5.19	6.35	-0.35	0.49, 0.04	0.71, 0.01	5.23, 0.04	6.43	0.08	-0.43
Mo(2)	0.51	0.62	5.14	6.27	-0.27	0.41, -0.10	0.67, 0.05	5.22, 0.08	6.30	0.03	-0.30
Sb	1.37	3.08	-	4.45	0.55	1.38, 0.01	3.14, 0.06	-	4.53	0.08	0.47
Li						1.90	0.58	-	2.47		0.53
Total η	5.96	12.71	10.33	29.00							
Δη											
Total [a] η						(5.71+2)[b]	13.58	9.71	31.00		
Δη						-0.25	0.87	-0.62			
Total [c] η						7.76	13.79	10.45	32.00		
Δη						0.05	0.21	0.74			

[a] Model for $LiMo_2SbS_2$ structure assuming no Li valence electron is present

[b] Model includes Li core electrons

[c] Calculation for $LiMo_2SbS_2$ structure assuming the Li valence electron is added back

Table S4. Mulliken population analysis per formula unit of the parent, η_i and intercalated, η_f compounds. Data shown correspond to: electron counts per orbital (*s*, *p*, *d*), the total valence electrons per crystal site, the change of population (Δη) after the intercalation and the associated charge transfer (δ).